CSIRO Publishing

International *Journal* of Wildland Fire

Scientific Journal of IAWF

VOLUME 11, 2002

International Association of Wildland Fire

IJWF is published for the International Association of Wildland Fire by:

CSIRO PUBLISHING
PO Box 1139 (150 Oxford Street)
Collingwood, Victoria 3066
Australia

Telephone: +61 3 9662 7644 (editorial enquiries)
+61 3 9662 7668 (subscription enquiries and claims)

Fax: +61 3 9662 7611 (editorial enquiries)
+61 3 9662 7555 (subscription enquiries and claims)

Email: publishing.ijwf@csiro.au (editorial enquiries)
publishing.sales@csiro.au (subscription enquiries and claims)

CSIRO PUBLISHING

Please submit all new manuscripts directly to **CSIRO** PUBLISHING, in electronic form only. See the *IJWF* Notice to Authors for more information.

www.publish.csiro.au/journals/ijwf

International Journal of Wildland Fire, 2002, **11**, 233–246

Studying wildfire behavior using FIRETEC

Rodman Linn[A,C], *Jon Reisner*[A], *Jonah J. Colman*[B] *and Judith Winterkamp*[A]

[A]Earth and Environmental Sciences Division, Los Alamos National Laboratory, Los Alamos, NM 87545, USA.
[B]Institute for Geophysics and Planetary Physics, Los Alamos National Laboratory, Los Alamos, NM 87545, USA.
[C]Corresponding author: Telephone: +1 505 665 6254; fax: +1 505 665 3415; email: rrl@lanl.gov

This paper is derived from a presentation at the 4th Fire and Forest Meteorology Conference, Reno, NV, USA, held 13–15 November 2001

Abstract. A coupled atmospheric/wildfire behavior model is described that utilizes physics-based process models to represent wildfire behavior. Five simulations are presented, four of which are highly idealized situations that are meant to illustrate some of the dependencies of the model on environmental conditions. The fifth simulation consists of a fire burning in complex terrain with non-homogeneous vegetation and realistic meteorological conditions. The simulated fire behavior develops out of the coupling of a set of very complex processes and not from prescribed rules based on empirical data. This represents a new direction in wildfire modeling that we believe will eventually help decision makers and land managers do their jobs more effectively.

Additional keywords: Los Alamos, New Mexico, simulation, modeling.

Introduction

Current wildfire models range in complexity from simple algebraic models that may be implemented in graphical form or on hand-held calculators to complex formulations that require vast computational resources. They also vary in origin from purely empirical formulations (Andrews 1986; Finney 1998) to physics-based algorithms (Grishin 1997; Dupuy and Larini 2000; Porterie *et al.* 2000; Grishin 2001*a*, 2001*b*) to combinations of the two (Clark *et al.* 1996; Coen and Clark 2000). These models of differing complexity and origin are appropriate for different applications based on the environmental conditions of the modeled fires, completeness of the available fuels and weather data, computational resources available, and urgency of the results. Many of the more complex models are not suitable for faster-than-real-time applications even on today's supercomputers. However, we postulate that their more physically based nature could make them better learning tools and allow them to be used to examine some of the more complex wildfire behaviors. In addition, not all field applications require faster-than-real-time output, such as planning, training, and risk assessment.

FIRETEC (Linn 1997) is a coupled atmospheric transport/wildfire behavior model being developed at Los Alamos National Laboratory, and is based on the principles of conservation of mass, momentum, and energy. FIRETEC represents the combined effects of the unresolved fine-scale process such as the convective heat transfer between solids and gases or the chemical reactions using simplified models that depend on resolved quantities such as average temperature and average surface area per unit volume. FIRETEC employs a fully compressible gas transport formulation to couple its physics-based wildfire model with the motions of the local atmosphere. FIRETEC can be run in a two- or three-dimensional mode. The three-dimensional version is beginning to be used to study wildfire–atmosphere interactions both in idealized and more realistic postulated or historical fire scenarios (Bossert *et al.* 2000). The studies are being performed to identify problems with and sensitivities of the model, as well as for validation purposes.

Some examples of the physical phenomena being studied are the effects of transient wind conditions, non-homogeneous terrain, non-uniform fuel beds with patchy distributions, and different vertical fuel structures. By studying the physical processes that drive wildfires, we hope to assist in the further development of the simpler models and identify situations where they are or are not appropriate for use or should be used with caution. Once properly validated, FIRETEC could be used to assist with decisions about fuel management strategies, and the implementation of controlled burns, under a variety of feasible scenarios.

 10.1071/WF02007 1049-8001/02/030233

FIRETEC is combined with the hydrodynamics model, HIGRAD (Reisner *et al.* 2000*a*), in order to simulate wildfires using a terrain-following three-dimensional finite volume grid. Current simulations typically utilize horizontal resolutions between 2 and 10 m and vertical resolutions between 0.6 and 6 m near the ground. Fuel moisture can be varied, fuel distributions can be tapered, and voids can be left between fuel stories. FIRETEC was developed as a framework of coupled process models that provide the capacity for a physics-based model capable of describing wildfire behavior in a wide variety of circumstances.

We believe that a three-dimensional wildfire model of this type could help us, as a society, to better cope with wildfires by providing another tool to be used in conjunction with currently implemented empirically-based models. The use of a model like FIRETEC, whose formulation and assumptions are completely different from empirically-based models, has significant benefits in some scenarios when used in parallel with faster running models. After models like FIRETEC have been refined and validated for simple scenarios, which has only just begun, it would be valuable to use these physics-based models alongside operational models for complex scenarios. It would add confidence in cases where there is good agreement and caution decision makers in other cases. It could also allow decision makers to study complex or severe burning conditions before events occur. This would help them to understand and avoid the evolution of potentially catastrophic situations, and assist in the development of fast-running models for these cases. There is much room for improvement of the physical-process models incorporated in FIRETEC, and it is not a replacement for other styles of wildfire models. However, the information provided in this text does provide encouraging evidence that there could be substantial future advancements in our ability to represent wildfire behavior through refinement of coupled-physical process models.

In this publication our goal is to illustrate the use of the combined HIGRAD/FIRETEC modeling system for examination of wildfire behavior. We will present examples of recent simulations performed with HIGRAD/FIRETEC in idealized situations as well as realistic conditions. A brief description of FIRETEC will be presented along with some discussion of these simulations and their significance. It is not our intention to give a comprehensive description of FIRETEC/HIGRAD here. Many of the details of FIRETEC, HIGRAD, and the numerical implementation thereof are described in other papers and reports (Linn 1997; Reisner *et al.* 2000*a*, 2000*b*). Furthermore, FIRETEC is a work in progress and we are well on the way towards improving the physical-process models and numerical implementation schemes incorporated in FIRETEC.

FIRETEC Model Description

The formulation of FIRETEC is based on representations of some of the physical processes that drive wildfires. This type of formulation gives FIRETEC a self-determining nature and adds to its generality. In this context, self-determining describes a model whose net predicted fire behavior (spread rate, intensity, fuel depletion, etc.) is determined by an evolving set of coupled physical processes that have both local and non-local space and time dependencies (such as the effects of distant topography, the preheating of fuel leading to fast ignition, and coupled atmosphere–fire interaction changing the shape of a fire line).

FIRETEC is an attempt to represent the average behavior of gases and fuels in the presence of wildfires. The precise local wind patterns caused by flow around particular fuel structures smaller than the spatial resolution of the model, or the instantaneous fluctuations in temperature produced by an individual lick of flame on a time scale smaller than the temporal resolution of the model, are not represented explicitly. Instead, FIRETEC describes the essence of the combination of many small-scale processes without describing each process in detail. The specific configurations of the small-scale solid structures (both fuel and terrain) are not available, and the initial and boundary conditions are known only as a set of average quantities. For example, the locations of individual branches or leaves are not known, so we use fuel characteristics such as average amount of fuel per unit volume. Likewise, the precise instantaneous velocities are not available for initial or boundary conditions, so we use average incoming velocities and turbulent kinetic energy.

The general approach taken in the development of FIRETEC was to divide the variables that occur in relevant conservation of mass, momentum, and energy equations into mean and fluctuating parts and then take ensemble averages of these equations. As a result of this process a number of correlations appear in the averaged equations and these present a need for additional modeling in order to achieve closure. The correlations represent the average combined effects of fluctuations in instantaneous local variables. In many cases the modeling of these correlations and the representation of unresolved fluctuations in physical properties is what enables FIRETEC to be applied to fires on a landscape scale. The variables that are described by the resulting set of partial differential equations are average physical quantities meant to describe the evolving averaged properties of the gases and solids within a ‘resolved volume’. For the purposes of these discussions, the term ‘resolved volume’ is used to describe the smallest volume for which we actually keep track of mean properties. Since we are only explicitly calculating average quantities over volumes that are much larger than actual combustion zones or individual fuel elements, we are not attempting to model ‘flames’ explicitly.

Instead we use quantities such as the average temperature of the solids and gases along with average species concentrations to estimate probable locations for combustion zones.

The set of chemical reactions occurring in a wildfire is extremely complex and has many intermediate transient species. For the initial FIRETEC model described by Linn (1997), the enormous set of chemical reactions was simplified to a small set of reactions involving wood pyrolysis and several solid–gas and gas–gas reactions. In addition, a further simplification for the chemical reactions was also described to consist of a single solid–gas reaction that is presented in equation (1) (nomenclature used in this paper is explained in the Appendix):

$$N_{wood}\left(wood\right)+N_{O_2}\left(oxygen\right)\rightarrow\left(products\right)+\left(heat\right) \quad (1)$$

The stoichiometric coefficients N_{wood} and N_{O_2} describe the net amount of wood and oxygen consumed through pyrolysis and all of the intermediate reactions when a unit mass of 'inert' products is formed. The values of these coefficients are estimated based on information given by Drysdale (1985). For the purposes of exploring the potentialities of transport-model based wildfire simulations on a landscape scale, we are presently utilizing this extremely simplified reaction model along with a reaction rate described by equation (2).

$$\mathrm{F_{wood}} = \rho_{\mathrm{wood}}\rho_{\mathrm{O_2}}\sigma\Pi \quad (2)$$

The turbulent diffusion coefficient, s, is calculated based on length scales corresponding to vegetation geometry and the turbulent kinetic energy (Linn 1997). The isotropic turbulent kinetic energy associated with three selected length scales is calculated with a separate transport equation for each length scale. These transport equations, which are discussed in detail in Linn (1997), include terms that represent creation of turbulence by velocity shear and canopy–wind interaction, energy exchange between scales, diffusion, and turbulence dissipation. The coefficient Π is itself a function of the stoichiometric coefficients, a probability distribution function for the temperature within the resolved volume, and the relative densities of the reactants, as described in detail in Linn (1997).

The philosophy behind this particular model is that the rate of pyrolysis is ultimately related to the heat flux to the solid wood, which is tied to the nearby gaseous reactions that are limited by the amount of oxygen. If either pyrolysing wood or oxygen is absent, the complex chain of chemical reactions is broken. We assume that the rates of the exothermic reactions in areas of active burning are limited by the rate at which reactants can be brought together in their correct proportions (mixing limited). We note that the dominant exothermic reactions involved in a fire involve oxidation of hydrocarbons by oxygen. Under the conditions experienced in a fire, areas of active burning (again these are not explicitly resolved but are handled by a probability distribution function for temperature) have extremely high reaction rates for these reactions. These regions are also where there are large positive fluxes of hydrocarbons due to pyrolysis, and so oxygen can become locally depleted. The production of carbon monoxide, soot and other aromatic structures (produced during hydrocarbon oxidation when there isn't sufficient oxygen to go all the way to CO_2 as the end product) pays testament to the fact that oxygen is limited in some regions of active burning within a fire. Thus the heat fluxes to the solids, and so the rate of pyrolysis, will ultimately be limited by mixing processes.

This is an extremely crude model, but for these initial tests with resolved volumes between 2.4 and 60 m^3 it is valuable to examine the consequences of such a crude model before refining it further to include the gaseous hydrocarbons explicitly. We confined our interest to the burning of fine fuel for the initial development of FIRETEC, but recognize that, along with the implementation of more complicated gas phase chemistry models, we will eventually need to address the consequences of the slower smoldering of the large fuels.

For the solid fuel as well as its associated moisture, conservation equations are used for the average properties of the substance within a space much larger that the fuel elements themselves, which we refer to as the resolved volume. The average mass of wood and moisture per unit resolved volume are described by the conservation equations (3) and (4) and the temperature of the solid by equation (5).

$$\frac{\partial\rho_{\mathrm{wood}}}{\partial t} = -N_{\mathrm{wood}}F_{\mathrm{wood}} \quad (3)$$

$$\frac{\partial\rho_{\mathrm{water}}}{\partial t} = -F_{\mathrm{water}} \quad (4)$$

$$\left(c_{\mathrm{p_{water}}}\rho_{\mathrm{water}}+c_{\mathrm{p_{wood}}}\rho_{\mathrm{wood}}\right)\frac{\partial T_s}{\partial t} = Q_{\mathrm{rad}}+ha_{\mathrm{v}}\left(T_{\mathrm{gas}}-T_{\mathrm{s}}\right)-F_{\mathrm{water}}\left(H_{\mathrm{water}}+c_{\mathrm{p_{water}}}T_{\mathrm{boil}}\right)+F_{\mathrm{wood}}\left(\Theta H_{\mathrm{wood}}-\mathrm{c}_{\mathrm{p_{wood}}}T_{\mathrm{wood}}N_{\mathrm{wood}}\right). \quad (5)$$

Equation (5) describes the evolution in the specific internal energy of the solid in terms of the temperature of the solid and the densities of the wood and liquid water. The processes that are represented in equation (5) include: the net thermal radiation heat flux to the solid at a given location, represented here by Q_{rad}; the convective heat exchange between the solid and gas, with a convective heat exchange coefficient derived from relations in Incorpera and Dewitt (1985); energy loss due to the evaporation of water; and the net energy generated by the combustion of wood pyrolysis products. Θ represents the fraction of heat released from the gas phase reactions that is deposited directly back to the solid; it is approximated by a linearly increasing function of the amount of wood that has burned. The increasing value of Θ with the fraction of fuel consumed is meant to be a crude representation of the fact that the primary nature of burning at a given location changes over time from flaming combustion, with much of the heat escaping with the gases, to smoldering combustion where catalysis and insulation by char and ash cause a larger proportion of the heat to be recaptured by the solid.

By dividing the local instantaneous variables into mean and fluctuating parts and taking ensemble averages of the equations, conservation equations for the average density of oxygen, ρ_{O_2}, the average density of the combined gas, ρ_{gas}, the average momentum of the combined gas per unit volume in the i direction, $\rho_{gas}u_i$, and the average potential temperature of the combined gas, θ, are formulated. The temporal evolution of oxygen is described in equation (6) and includes terms to represent advection, turbulent diffusion, and depletion due to the combustion of wood pyrolysis products:

$$\frac{\partial \rho_{O_2}}{\partial t} + \frac{\partial u_i \rho_{O_2}}{\partial x_i} = \frac{\partial}{\partial x_j}\left(\sigma \frac{\partial \frac{\rho_{O_2}}{\rho_{gas}}}{\partial x_j} \right) - F_{wood} N_{O_2}. \qquad (6)$$

The density of the combined gas is calculated using equation (7), which can be thought of as the sum of the conservation equations of all gas phase species present.

$$\frac{\partial \rho_{gas}}{\partial t} + \frac{\partial u_i \rho_{gas}}{\partial x_i} = F_{wood} N_{wood} + F_{water}. \qquad (7)$$

The overall conservation of momentum is described by equation (8):

$$\frac{\partial \rho_{gas} u_i}{\partial t} + \frac{\partial u_i u_j \rho_{gas}}{\partial x_j} = -\frac{\partial R_{ij}}{\partial x_j} - \frac{\partial p}{\partial x_i} + \rho_{gas} g_i - \frac{3 C_D \rho_{wood} \rho_{gas} |u| u_i}{8 s_s \rho_{wood(micro)}} \qquad (8)$$

The terms to the right of the transport equation are advection, gradients of the turbulent Reynolds stress, gradients in pressure, buoyancy, and drag. The formulation of the non-isotropic Reynolds stress components is described in detail in Linn (1997) in terms of a Boussinesq approximation that depends on the prescribed length scales, velocity strain rates, and the turbulent kinetic energies associated with the length scales. The drag term depends on the ratio of the mass of wood per resolved volume to the microscopic density of the wood (the volume fraction), on the density of the gas, and on the speed and velocity of the gas. The size scale, s_s (representing the average size of the fuel elements), and the volume fraction give this term flexibility to handle different fuel loads and configurations. The value of the drag coefficient, C_D, is currently estimated to be near unity based on cylindrical fuel elements and relevant Reynolds numbers as described in Fox and McDonald (1985). Different values of C_D would be appropriate for other fuel element shapes and more extreme values of R_{ij}. Both the appropriate drag term and the value of C_D, and their respective dependence on fuel configuration, are the subjects of ongoing research.

Equation (9) describes the evolution of the potential temperature of the combined gas using advection, turbulent diffusion, and source terms. The source term in equation (9) represents the combination of convective heat exchange (mirroring the convective heat exchange term in equation 5), radiative heat, and an energy source from the chemical reactions:

$$\frac{\partial \rho_{gas} \theta}{\partial t} + \frac{\partial \theta u_j \rho_{gas}}{\partial x_j} = \frac{\partial}{\partial x_j}\left(\sigma \frac{\partial \theta}{\partial x_j} \right) + \frac{\theta}{c_p} \left[\frac{h a_v \left(T_s - T_{gas} \right) + Q_{rad,gas} + F_{wood} \left(1 - \Theta \right) H_{wood}}{T_{gas}} \right]. \qquad (9)$$

$Q_{rad,\,gas}$ represents the net gain of energy by the gas from thermal radiation. $Q_{rad,\,gas}$ is calculated based on a two-field thermal radiation scheme, adapted from Stephens (1984), that utilizes a three-dimensional diffusional transport approximation tailored for thermal heat transfer through a medium which may be optically thin. Energy is emitted or absorbed from the gas phase based on a probability distribution function for gaseous temperature and species concentrations. The emitted energy is diffused through the gaseous media based on a radiation energy density that is not tied to the temperature of the gas and is absorbed by solid objects based on their projected surface area per unit volume. This transport formulation is not as accurate as discrete transfer methods (Baum and Mell 1998) but is less computationally expensive.

Simulations

In this section several simulations are described in order to illustrate the use of a physics-based transport model like FIRETEC for studying wildfire behavior. The first four simulations described are very simple idealized fire scenarios that we present to illustrate our ability to examine the dependence of fire behavior on fuel and atmospheric conditions. The last simulation described in this section consists of a fire burning in complex terrain with non-homogeneous vegetation and realistic meteorological conditions in order to illustrate the use of FIRETEC in complex conditions.

Simulation 1 consists of a fire ignited in the middle of a 160 m × 160 m homogeneous fuel bed with no ambient wind present. The general layout for simulation 1 is shown in Fig. 1. The fuel was specified such that it had characteristics similar to tall grass. However, because we are not using the standard Anderson fuel models, the fuel bed is not exactly the same as one that would be specified for BEHAVE (Andrews 1986). The characteristics for fuel beds in FIRETEC are not confined to any predetermined or pre-established fuel models and could be derived directly from fuel measurements if available. The FIRETEC fuel-bed characteristics chosen for these simulations include fuel height of 0.7 m, a fuel density of 1 kg/m^3 within the fuel bed, a surface area per unit volume of fuel of 4000 m^{-1}, and a heat of combustion of 8914 kJ/kg estimated from Drysdale (1985). These values represent user chosen inputs that were chosen to be representative of a tall grass field (similar to the fuel described by Anderson fuel model 3). This heat of combustion is an estimate based on values for fine wood.

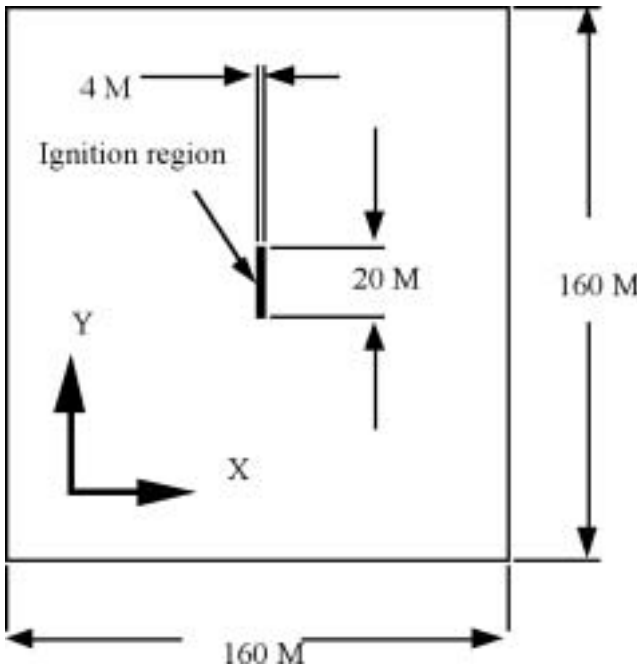

Fig. 1. Basic layout of the simulations 1, 2, and 3 at the time of ignition.

In order to further tailor this simulation for grass in the future, we might need to alter this heat of combustion to reflect the different chemical makeup of grass from other foliage. The fuel moisture fraction in simulation 1 is initially set to be 0.05 (fuel moisture fraction being defined as the mass of the water divided by the mass of the fuel). Because the vertical resolution near the ground in this simulation is approximately 1.5 m, the fuel exists only in the layer of finite difference cells nearest to the ground. The atmospheric conditions (i.e. the ambient winds) are initially still with neutral atmospheric stability. As time progresses, the air within the domain moves under the action of the fire while the boundary velocities and stability are held fixed. These boundary conditions are not believed to influence the fire behavior in this simulation significantly.

The ignition of the fire is achieved by removing any fuel moisture and steadily raising the mean temperature of the fuel within a 4 m × 20 m box (see Fig. 1) from 300 K to 500 K over 1 s. This is a very fast ignition and causes intense burning at the beginning of the simulation, but the model quickly compensates for this abrupt insertion of energy. As the fire burns outward from its rectangular ignition area it becomes less elongated because the fire spreads normal to the long side at speeds equal to or greater than the spread rates normal to the short sides. The preheating is slightly greater near the middle of the long sides of the rectangular ignition area than along the short sides because of the effects of the higher radiation view factors being felt. At later times the fire perimeter starts to have irregularities that are caused by the interaction between the fire and the atmosphere. In some locations the fire-induced updraft draws enough cold air across the perimeter that the fire is significantly damped in that location.

An example of this is shown in Fig. 2. In some cases the fireline is able to 'heal' itself and in some cases this damping is sufficient that the perimeter is permanently broken. This simulation is allowed to burn for 300 s at which time the fire has progressed approximately 24 m from the ignition area in one direction. The eventual spread rate of the fire in the positive x direction is approximately 0.05 m/s. This spread rate is slightly faster than the spread rate predicted by BEHAVE for a no-wind fire in standard fuel model 3 (tall grass) with 0.05 moisture fraction (~0.03 m/s). We do not expect these spread rates to be equal based on differences in the fuel bed that we prescribed versus the fuel that fuel model 3 actually represents. The surface area of the fuel, the shape of the fuel, and the average load have a significant effect on the fire behavior. During this particular simulation the updrafts were often on the order of 10 m/s. Three isosurfaces, which define relative levels of a combination of gas temperature and oxygen depletion, along with fuel depletion color contours, are used to visualize simulation 1 at 100 and 200 s after ignition in Fig. 2.

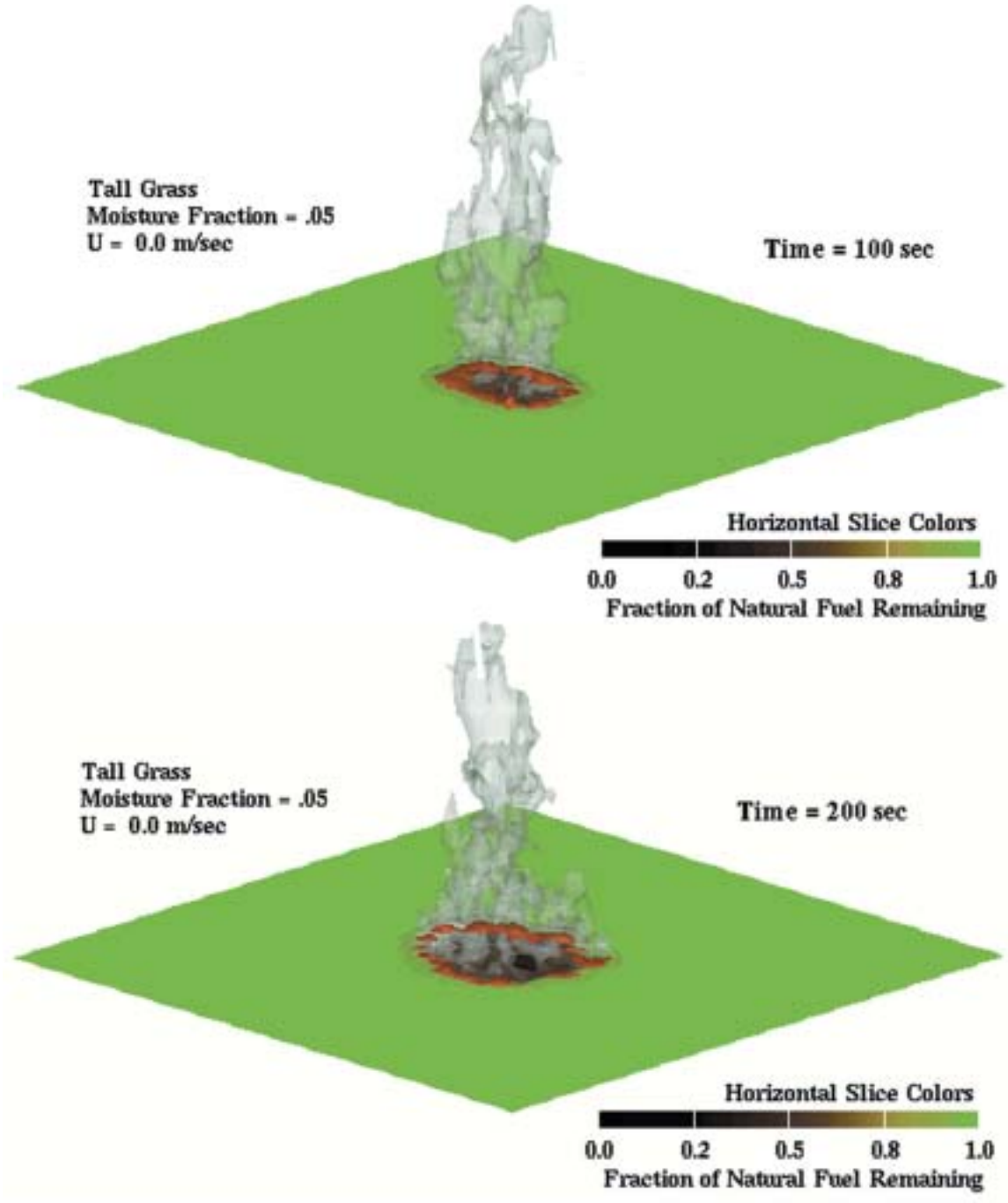

Fig. 2. Oblique views of simulation 1 shown at 100 and 200 s after ignition. The red, orange, and gray isosurfaces indicate the locations of decreasing levels of heated gas emissions as described in the text. The horizontal surface contains color contours indicating fuel depletion (green indicates initial fuel load and black indicates fine fuel depletion.)

The complex flow structure involved in the fire plume can be illustrated using isosurfaces of vertical vorticity. Fig. 3 contains isosurfaces of positive and negative vorticity values (1.2 s^{-1} for the white isosurface and –1.2 s^{-1} for the black isosurface) and horizontal wind vectors (maximum length of vector represents 2 m/s) just above the fuel bed. The vectors show the strong inflow of air near the base. This inflow contributes to the convective cooling of the ground fuels outside of the fire perimeter. This convective cooling must be overcome by the radiative heating of the fuel in order for the fire to propagate. The vortices are the cause of the broken perimeter discussed above as they force a relative

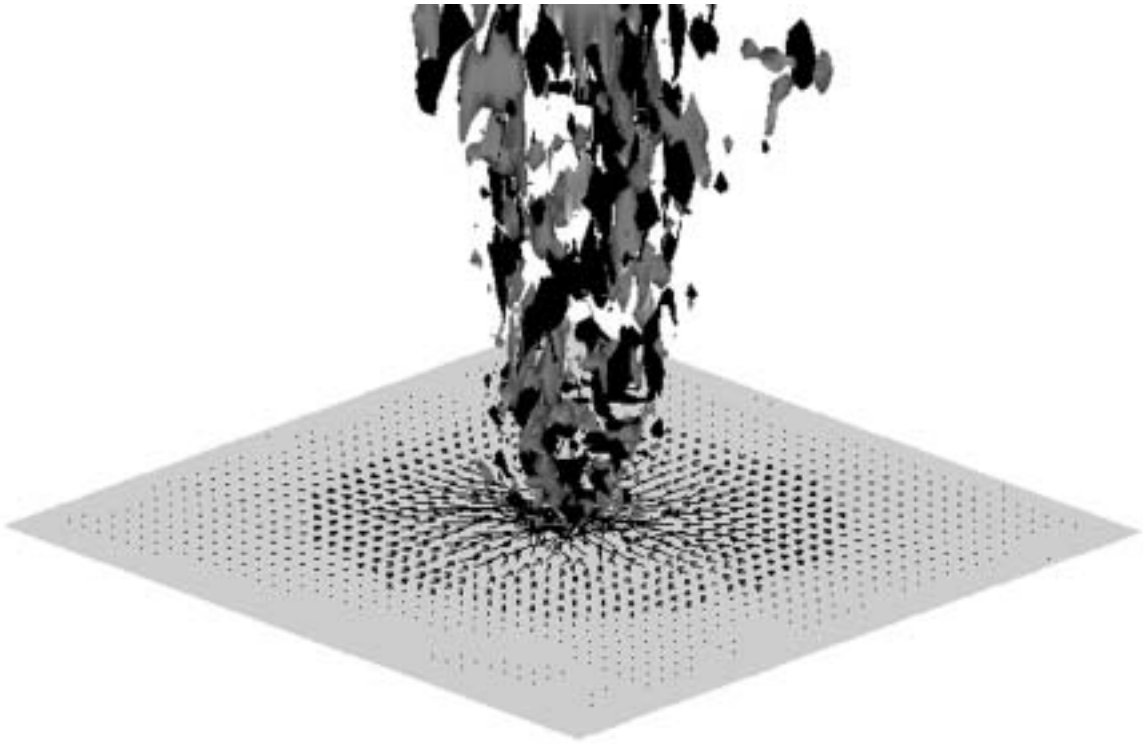

Fig. 3. Oblique views of simulation 1 shown at 200 s after ignition. The gray and black isosurfaces indicate regions where the vertical vorticity is 1.2 s^{-1} and –1.2 s^{-1}. The gray plane indicates the location of the fuel bed and the vectors represent horizontal component of velocities just above the fuel bed. The horizontal velocity component at this elevation is ~2 m/s.

increase or decrease in flow between locations of positive and negative vorticity. Physics-based fire models like FIRETEC can provide information about how the complex interaction between fires and the atmosphere affect the fire behavior.

Simulation 2 consists of a fire ignited in almost identical circumstances to the fire in simulation 1, the difference being that the initial fuel moisture fraction is 0.30 in simulation 2 instead of the 0.05 in simulation 1. Because we ignite the fuel by first drying it and then forcing its average temperature up to 500 K, any fuel within the initial 40 m^2 rectangular region (Fig. 1) will burn until depleted. The fire propagates out of its initial region due to the rate and intensity of the fire within the initial region but, as the fire moves into the wetter fuel, it propagates at a slower rate because it is losing energy to moisture evaporation. Eventually the fuel within the initial perimeter burns out and the fire begins to lose intensity. After approximately 75 s, the perimeter of the fire becomes significantly broken. After approximately 200 s, there is essentially no forward progress by the fire front and the fire has only a few points around the perimeter that have not gone out. The fire from simulation 2, 200 s after ignition, is depicted in the top image of Fig. 4. When this image is compared with the second image in Fig. 2, it is easy to see the reduction in spread distance and intensity caused by the increase in moisture.

Simulation 3 begins exactly the same as simulation 1. Then, after 100 s of simulated time, the ambient winds are increased to 6 m/s in the positive x direction over 6 s and then held constant for the remainder of the simulation. The change in the ambient wind speed causes the fire to change character significantly. The fire's first response to the change in wind speed is to lay over in the downwind direction. Much of the plume of heated air is carried downwind and remains closer to the ground than it had under the no-wind conditions. As the ambient wind blows cool air into the upwind side of the elliptical fire line it pushes the heat away from the unburned fuel in this region and the fire on the upwind side begins to lose intensity. The fuel upwind of the elliptical fire perimeter no longer gets as much preheating as it did in the no-wind condition because the heat is being convected away from the unburned fuel, the radiation view factor to this fuel is decreased, and the ambient wind is blowing more cool air over the previously preheated region (thus causing convective cooling). This part of the elliptical fire perimeter can be thought of as acting like a backing fire trying to move against a 6 m/s wind and its progress is essentially stopped.

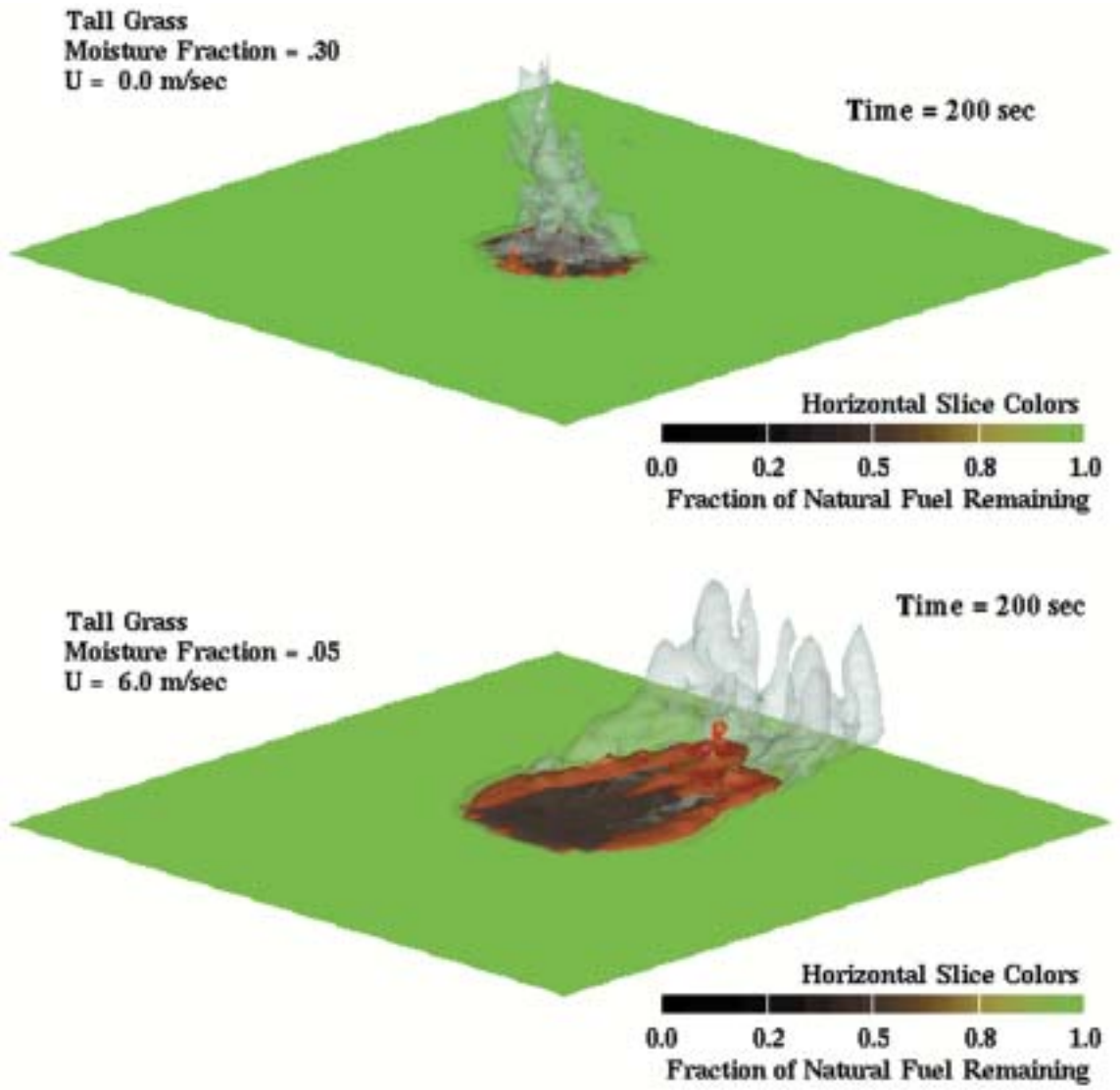

Fig. 4. Oblique views of simulations 2 and 3 shown at 200 s after ignition. The red, orange, and gray isosurfaces indicate the locations of decreasing levels of heated gas emissions as described in the text. The horizontal surface contains color contours indicating fuel depletion (green indicates initial fuel load and black indicates fine fuel depletion.)

When the ambient wind is increased the downwind portion of the elliptical fire perimeter is burning in the direction of the wind (acting as a heading fire) and begins to increase in intensity. The ambient wind pushes the heat generated by this portion of the fire closer to the unburned fuel. The fuel downwind of this portion of the fire is being preheated more due to the increased convective heat exchange and increased radiation view factor effects. As this preheated fuel ignites it widens the fire line and thus increases the buoyant force of the plume. The fuel line width appears to reach a maximum thickness due to the balance of fuel depletion on the upwind side of the line and the effect of the increasing buoyancy raising the plume and thus reducing the convective heat exchange to the downwind fuel. The spread rate of the fire in the downwind direction increases to a rate of approximately 1 m/s. The fire is allowed to burn for 205 simulated seconds, at which time the fire gets close enough to the boundary to potentially be affected by boundary conditions. This spread rate is slower than the steady state spread rate that would be calculated using BEHAVE for a line fire driven by a 6 m/s wind in fuel type 3 (~2.5 m/s). This difference is not unexpected since the fire in simulation 3 is still accelerating and this spot fire is not expected to move as fast as a BEHAVE line fire even at an approximate steady state.

Simulation 4 consists of a fire ignited from a similar 40 m^2 rectangular area on dry grass (fuel moisture fraction of 0.05) and blown towards a 'forest' that has a grass understory, no ladder fuels, and a 0.20 kg/m^3 extremely dry crown (combined live and dead fuel with a composite moisture fraction of 0.80). This low fuel moisture was chosen to represent a fuel canopy that was extremely stressed and has some dead fuel intermixed. In this simulation the location of the ignition area is shifted 15 m in the negative x direction compared with what is shown in Fig. 1, in order to provide more room for the fire to develop while approaching the 'forest' region. The winds are ramped up from 0.0 m/s to 3.0 m/s over the first 40 s after ignition. The crown was configured such that the height to the base of the crown was 5 m and the height to the top of the crown was 10.6 m. The bulk density of the crown was assumed to have a uniform distribution for simplicity. There are essentially no ladder fuels in this simulation within the gap between the grass and the crown.

The fire in simulation 4 burns only in ground fuels for approximately 120 s, at which time the fire begins to consume some of the crown fuel. During the first 120 s the spread rate reaches approximately 1 m/s, which is similar to the spread rate predicted by BEHAVE for a fire in fuel model 3, winds of 3 m/s, and fuel moisture fraction of 0.05 (1.04 m/s). In order for the crown fuels to ignite, the convective and radiative heat transfer from the ground fire must overcome the convective cooling of the crown caused by the ambient wind through the crown and the entrainment of cooler air from above and below the crown. Due to the 4.3 m stem space between the ground fuels and the canopy where there is no fine fuel present in this simulation, there is a flow of air between the ground fuels and the canopy. This supply of air continues to drive the ground fire. In addition, any fire that reaches the crown can easily draw air from below the crown; this promotes vertical advection of heat instead of lateral diffusion (vertical wind speeds through the crown reach 13 m/s). This chimney effect can be contrasted to the vertical velocities within the fuel bed of the grass fire, which are much lower (approximately 3 m/s) due to the inability to draw air from below the fuel.

In this simulation there is only enough sustained heat flux to the crown fuels to sporadically burn the fuel. There is enough cooling in this configuration to allow spotty torching of the crown but not a sustained crown fire that consumes all of the crown fuels. Although we have not extensively examined the sensitivities of the transition to crowning and production of self-sustaining crown fires as other researchers have done (Albini and Stocks 1986), we believe that, after refinement and validation, simulations like this one might be capable of assisting researchers who study crown fires, the thresholds that control them, and thinning strategies.

Figure 5 shows the fire in simulation 4 as it burns under the crown and occasionally burns up into the crown. In this figure the flat color contour slice that covers the entire domain uses colors to describe the depletion of the ground level fuels as seen in Figs 2 and 4. The darker green envelope which is offset from the ground is an isosurface describing the locations where at least 75% of the initial crown mass (combination of remaining fuel and moisture) remains. This broken-up isosurface shows that there are significant pockets of crown fuel that remain intact after the front has past underneath them. We can see the ground fire still burning under the crown if we look through the holes in the crown isosurface.

We compare the distances that the fires spread along the positive x direction for simulations 1, 2, 3, and 4 in Fig. 6. In this figure we see that, as expected, the fire in simulation 2 (with higher fuel moisture) progresses much more slowly than the fire in simulation 1 and eventually stops making progress after approximately 200 s. Figure 6 also shows that, after 100 s (the time when the ambient wind is increased in simulation 3), the spread rate of the fire in simulation 3 increases significantly. For the purposes of generating this plot a threshold temperature of 500 K was chosen.

In order to examine the distance that the various simulated fires traveled, we searched for the cell that had an average solid fuel temperature above 500 K and was farthest in the x positive direction from the ignition point. This was a simple way of defining a 'front' for examination of propagation. Due to the way the 'front' was defined we get occasional incidences where the temperature in a cell will heat up then cool down and reheat. This makes the curves in Fig. 6 appear as if the front retreats momentarily when in reality the fire is not moving back over itself; we are just seeing an artifact of the chosen diagnostics. It is thought that sudden cool gusts of air across the fire front cause this effect through convective cooling of the fuel. The points corresponding to simulation 4 describe the effect of increasing the wind to 3 m/s immediately after ignition and then a change in spread rate when the fire reached the crown. As the fire moves under the crown the drag of the canopy changes the nature of the ambient wind that reaches the ground fire front.

The curves for simulations 3 and 4 in Fig. 5 show nearly constant spread rates at late times in the simulations. The balance of the physical processes such as convective heat exchange, radiative heat transfer, vegetation drag, turbulence generation, and combustion processes appear to have established a stochastically average balance with one another. Investigation of balances such as these, which cause apparent steady state propagation rates, is one of the uses for this type of model in the future. The steady state propagation rate is an assumption in models like BEHAVE, whereas it is a result in FIRETEC.

A fifth simulation was performed for the sole purpose of illustrating the use of FIRETEC on a larger and more complex scenario. Simulation 5 consists of a simulated fire positioned in the lower left corner of a 1.28 km × 1.28 km region of Los

Alamos National Laboratory (LANL) in the foothills of the Jemez Mountains in New Mexico. This particular region was chosen for this simulation based on its perceived vulnerability to wildfires in April 2000. The simulation was run in late April 2000 just prior to the time when this same piece of land was burned during the Cerro Grande fire. LANL personnel had done extensive fuels inventory mapping as a part of an effort for the U.S. Department of Agriculture (USDA) Forest Service–Rocky Mountain Research Station.

Ground level fuel loads for this region are shown in Fig. 7. Fuel conditions (such as fuel moisture) and meteorological conditions were derived from the local fuel and meteorological conditions present during the Oso complex fire, which occurred during the summer of 1999 approximately 6 miles away. These were chosen in order to use a realistic and consistent set of conditions for a wildfire in this geographic area. The ambient winds near the ground were specified as approximately 2.5 m/s and blowing from the south-west corner of the domain towards the north-east corner. However, the terrain is rather complex and the presence of mountains to the west, along with a narrow canyon running east–west through the domain, cause the ground level winds to be quite variable within the domain.

The fire was ignited within a 40 m × 40 m area near a road intersection in the south-west corner. The fire began burning down a gentle slope to the north-east until it reached the narrow canyon, where it slowed significantly as it burned down into the canyon. This reduction in speed caused by the downslope is not prescribed by a rule in FIRETEC as it would be in a purely empirical model. This deceleration occurs because the radiation view factor, and the convective heat transfer, to the unburned fuel decrease as the angle between the heated plume and the ground increases. It took approximately 24 min from the time of ignition to get to the bottom of the canyon (as seen in the top panel of Fig. 8). The cumulatively averaged spread rate during this period was approximately 0.4 m/s.

During the first 24 min the fire was burning mostly through regions of Ponderosa Forest and Pinon Juniper. The bottom panel of Fig. 8 depicts the fire 36 min after ignition. Between 24 and 36 min after ignition the fire moved at a much faster pace (12 min averaged spread rate of approximately 1.4 m/s) than it had during the first 24 min. One factor leading to the faster spread rate is the fire accelerating up the side of the canyon as a result of the increased radiation view factor and the plume being pulled

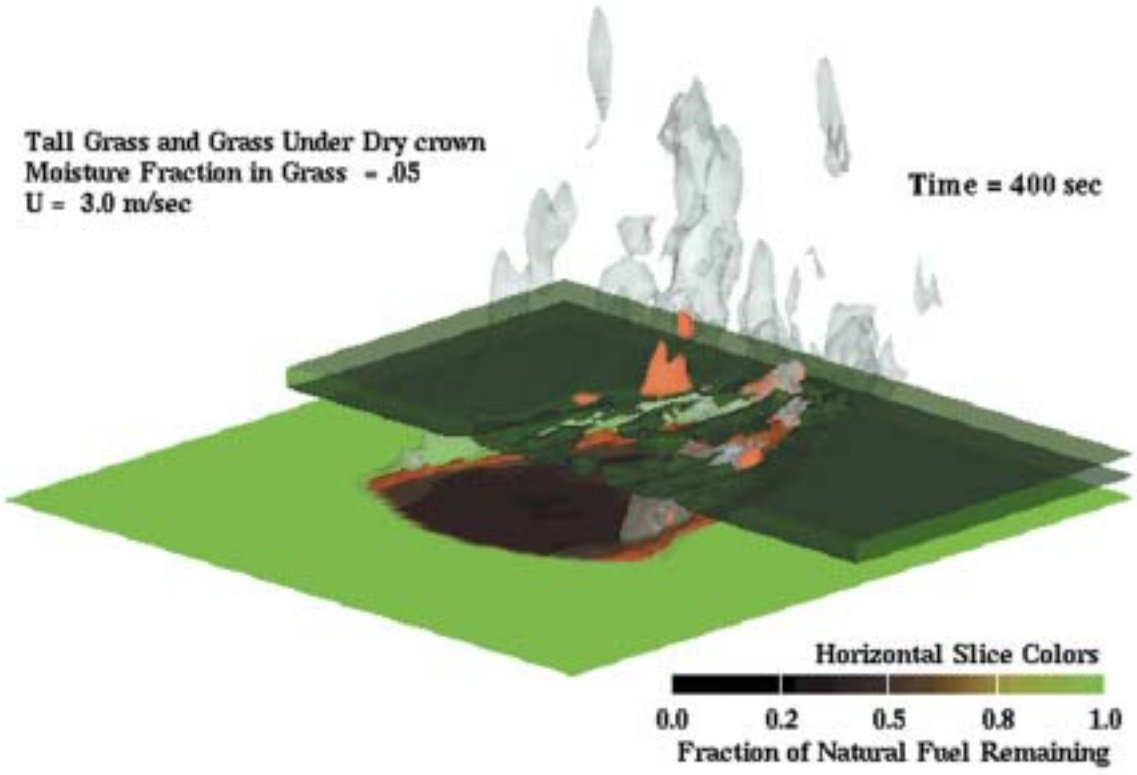

Fig. 5. An oblique view of the crown fire from simulation 4 shown at 200 s after ignition. The red, orange, and gray isosurfaces indicate the locations of decreasing levels of heated gas emissions as described in the text. The horizontal surface contains color contours indicating fuel depletion (light green indicates initial fuel load and black indicated fine fuel depletion.). The dark green envelope which is offset from the ground is an isosurface describing the locations where at least 75% of the initial crown mass (combination of remaining fuel and moisture) remains.

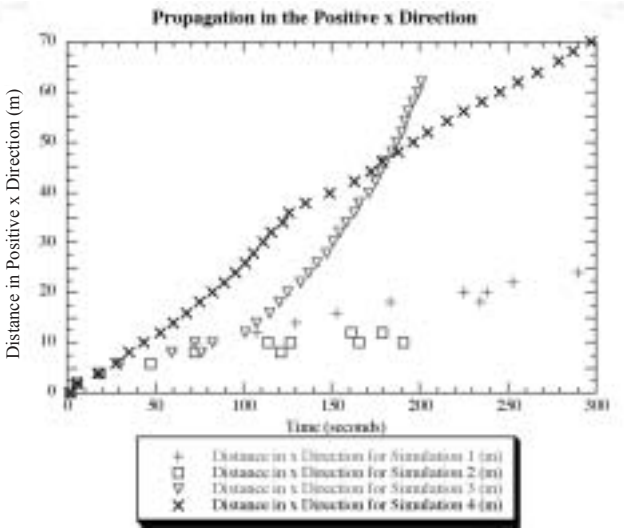

Fig. 6. Propagation distances in the positive x direction for simulations 1, 2, 3, and 4.

closer to the unburned fuel, thus increasing the convective heat transfer. Another factor was that the fire then moved out of the thicker vegetation onto a gentle upslope of thin dry grass (shown in blue in Fig. 7.) The fire moved across the grass very quickly, but depleted the fuel in that area quickly as well (shown by the large black region surrounded by fire in the bottom panel of Fig. 8). Other areas that had heavier fuel loads and more aerodynamic drag allowed the fire to burn for much longer periods of time. The cumulative effective spread rate for the fire moving across the entire domain was approximately 0.75 m/s.

Conclusions

In this brief description of HIGRAD/FIRETEC, and of five simulations that utilized it to represent wildfire behavior in idealized and realistic situations, we tried to give the reader a sense of the types of calculations and studies that are possible with a physics-based wildfire model. In comparison to large fires, all of the simulations presented here are relatively small in geographical size. However, at this point we are focused on learning how to capture the driving physical processes, most of which are very small in scale compared with extensive fires. By modeling the driving physical processes, we can examine their complex interaction in order to learn more about the sensitivities of wildfires to various environmental conditions. By understanding more of these sensitivities we hope to assist in developing the simple models.

FIRETEC has been used to perform a number of different simulations in conjunction with the atmospheric hydrodynamics model HIGRAD. Four idealized simulations are shown here for the purpose of illustrating the behavior of FIRETEC in very simple scenarios and to point out some of the dependencies of the model on environmental conditions. The results of these simulations are not unexpected or novel but the use of a physics-based full-transport model to perform the simulations represents the initial development of

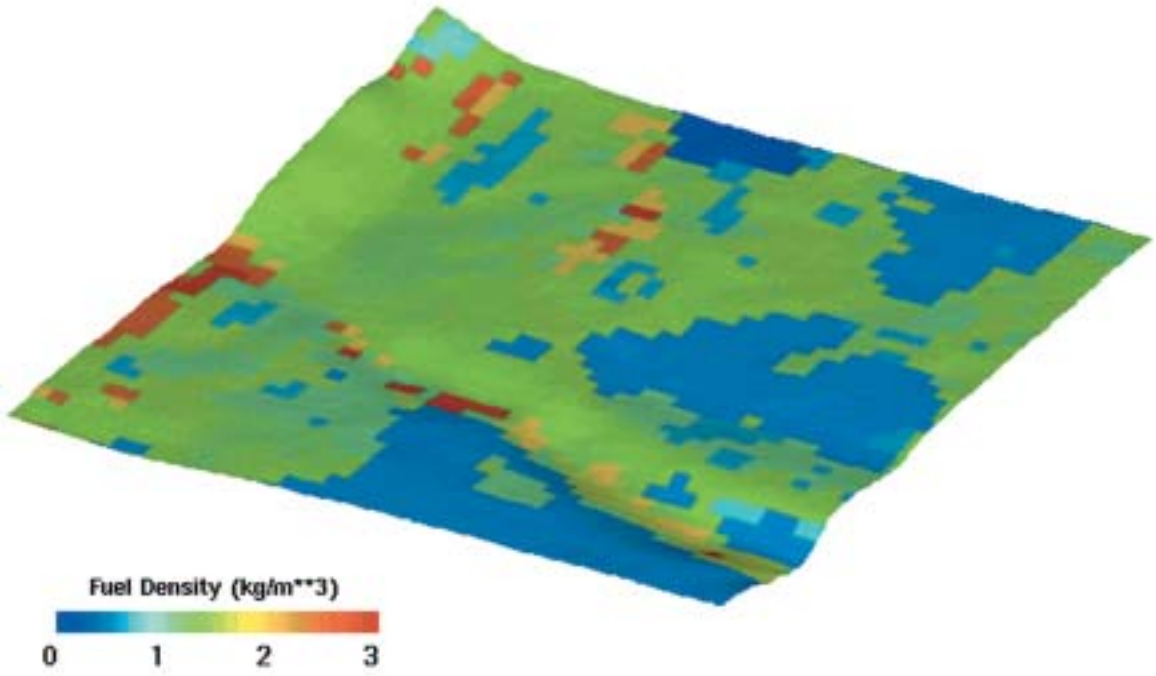

Fig. 7. Ground level fuel densities for simulation 4.

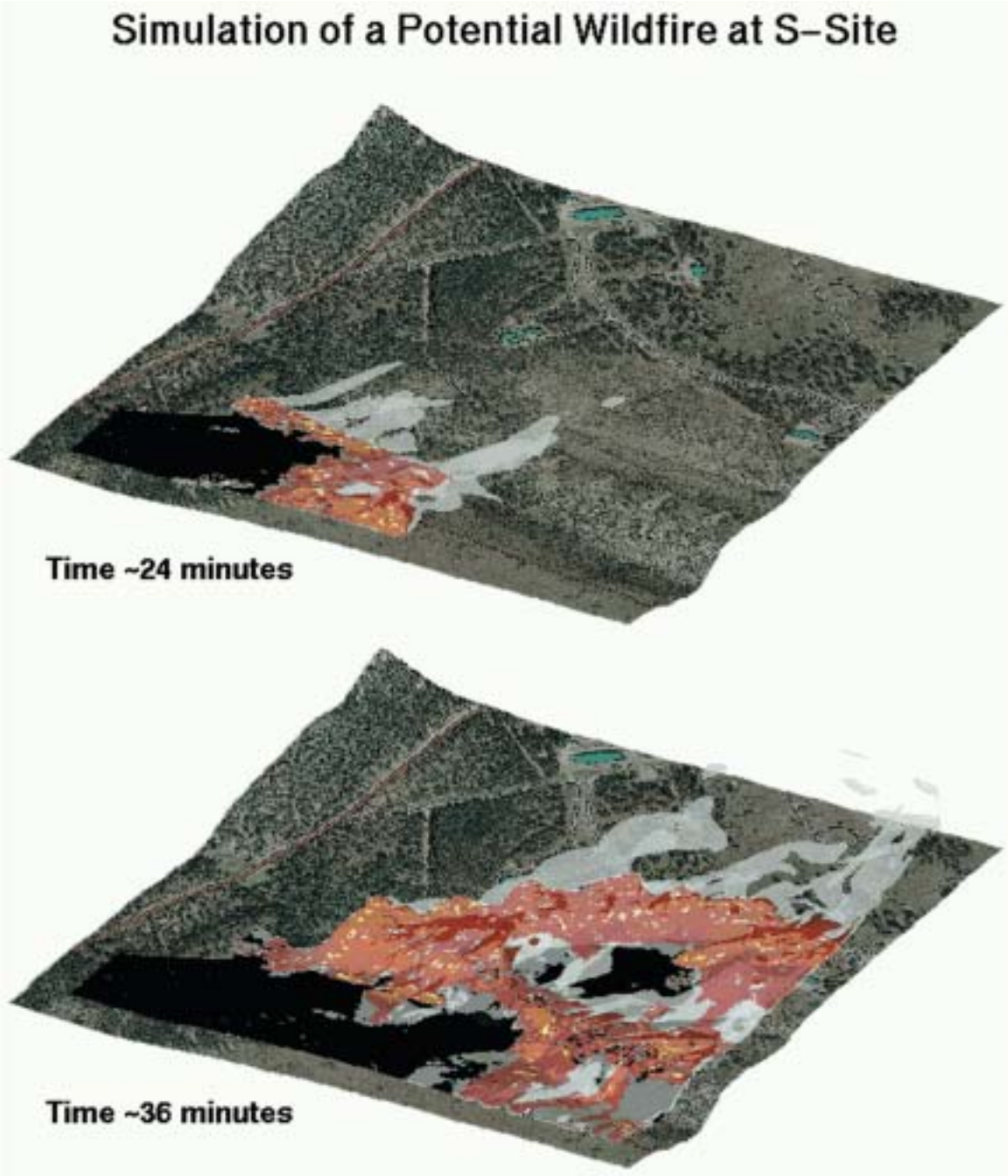

Fig. 8. The position of the fire in simulation 5 at times of 24 and 36 min using yellow, red, and gray isotherms to represent regions there the potential temperature is above 500 K, 350 K, and 310 K respectively. The black area behind the fire is area where the fuel has been depleted.

a new avenue in landscape-scale wildfire modeling. The simplicity of these idealized simulations allows us to isolate some of the physical relationships that cause the simulated fires to act the way that they do. Many of the cause and effect relationships agree with intuition, but the important point is that these relationships developed out of the coupling of a set of very complex processes and not from prescribed rules based on empirical data.

This subtle difference is what sets this type of model apart as a self-determining model and a different approach to wildfire modeling. We have simulated a number of more realistic fires with HIGRAD/FIRETEC, some historic and

some postulated. One of the realistic postulated fires is described within this paper. Although it is impossible to validate the model against a fictitious fire, we are encouraged by the reasonable spread rates and fire behavior in the vicinity of upslopes, downslopes, and non-homogeneous fuels.

By exploring new research avenues in wildfire modeling, we believe that we will eventually help decision makers and land managers do their jobs more effectively. Models like FIRETEC will never replace fast-running operational models like BEHAVE or FARSITE (Finney 1998) but it is our hope that they will eventually assist in the further development of some of these models and add a novel way of examining complex scenarios for research purposes or land management. Our philosophy for future development of this model is to work on finding ways to validate the behaviors that FIRETEC produces in simple scenarios and explore new ways of accurately representing the numerous physical processes that are important for determining wildfire behavior. This model is in the early stages of its development and, by working to find ways of validating FIRETEC, we will undoubtedly find that there are process models that are missing or need improvements. By striving to be able to capture wildfire behavior in simple scenarios, we will concurrently develop confidence in the model's ability to represent complex scenarios because we will have developed confidence in the underlying process representations.

Acknowledgements

We thank the IGPP for timely support of this project over the years, LANL for contributions to this work through the LDRD program, and Frank Harlow for significant contributions to FIRETEC's development.

References

Albini FA, Stocks BJ (1986) Predicted and observed rates of spread of crown fires in immature Jack Pine. *Combustion Science and Technology* **48**, 65–76.

Andrews PL (1986) BEHAVE: fire behavior prediciton and fuel modeling system–BURN subsystem, Part 1. USDA Forest Service, Intermountain Research Station General Technical Report INT–194. Ogden, UT. 130 pp.

Baum HR, Mell WE (1998) A radiative transport model for large-eddy fire simulations. *Combustion Theory Modeling* **2**, 405–422.

Bossert JE, Linn RR, Reisner JM, Winterkamp JL, Dennison P, Roberts D (2000) Coupled atmosphere–fire behavior model sensitivity to spatial fuel characterization. In 'Proceedings of the Third Symposium on Fire and Forest Meteorology', January 2000, Long Beach, CA.

Clark TL, Jenkins MA, Coen J, Packham D (1996) A coupled atmosphere–fire model: convective feedback on fire line dynamics. *Journal of Applied Meteorology* **35**, 875–901.

Coen JL, Clark TL (2000) Coupled atmosphere–fire model dynamics of a fireline crossing a hill. In 'Proceedings of the Third Symposium on Fire and Forest Meteorology', January 2000, Long Beach, CA.

Dupuy, J-L, Larini M (2000) Fire spread through a porous forest fuel bed: A radiative and convective model including fire-induced flow effects. *International Journal of Wildland Fire* **9**, 155–172.

Drysdale D (1985) 'An introduction to fire dynamics.' (John Wiley–Department of Fire Safety Engineering at the University of Edinburgh)

Finney MA (1998) FARSITE: Fire area simulator–model development and evaluation. USDA Forest Service, Rocky Mountain Research Station Research Paper RMRS-RP-4. Ogden, UT. 47 pp.

Fox RW, McDonald At (1985) 'Introduction to fluid mechanics.' (John Wiley–School of Mechanical Engineering at Purdue)

Grishin AM (1997) `Mathematical modelling of forest fires and new methods for fighting them.' (Publishing House of the Tomsk State University: Tomsk)

Grishin AM (2001*a*) Heat and mass transfer and modeling and prediction of environmental catastrophes. *Journal of Engineering Physics and Thermophysics* **74**, 895–903.

Grishin AM (2001*b*) Conjugate problems of heat and mass exchange and the physicomathematical theory of forest fires. *Journal of Engineering Physics and Thermophysics* **74**, 904–911.

Incorpera FP, DeWitt DP (1985) 'Fundamentals of heat and mass transfer.' (John Wiley–School of Mechanical Engineering at Purdue)

Linn RR (1997) Transport model for prediction of wildfire behavior. Los Alamos National Laboratory, Scientific Report LA13334-T.

Porterie, B, Loraud JC, Morvan D, Larini M (2000) A numerical study of buoyant plumes in cross-flow conditions. *International Journal of Wildland Fire* **9**, 101–108.

Reisner J, Wynne S, Margolin L, and Linn R (2000*a*) Coupled atmospheric–fire modeling employing the method of averages. *Monthly Weather Review* **128**, 3683–3691.

Reisner JM, Knoll DA, Mousseau VA, Linn RR (2000*b*) New numerical approaches for coupled atmosphere–fire models. In 'Proceedings of the Third Symposium on Fire and Forest Meteorology', January 2000, Long Beach, CA.

Stephens GL (1984) The parameterization of radiation for numerical weather prediction and climate models. *Monthly Weather Review* **112**, 827–867.

See over page for Appendix

Appendix. Nomenclature used in the text (in order of appearance)

Symbol	Description	Units
N_x	The ratio of the mass of the species x to the total mass of the combined products	Unitless
F_x	The rate of change of species x within a resolved volume.	Mass/(volume*time)
ρ_x	The density of species x within a resolved volume	Mass/volume
σ	The turbulent diffusion coefficient	Volume/(mass*time)
Π	The fuel rate of change coefficient, combining the temperature probability distribution function and the stoichiometry terms.	Unitless
C_{p_x}	The isobaric heat capacity of species x	Energy/(mass*temperature)
T_x	The average temperature of species x within a resolved volume.	Temperature
Q_{rad}	The net thermal radiation heat flux to the solid at a given location.	Energy/(volume*time)
h	The convective heat exchange coefficient.	Energy/(area*temperature*time)
a_v	The contact area per unit volume between the gas and the solid.	Distance
H_x	The heat energy per unit mass associated with a flux in species x.	energy/mass
Θ	The fraction of heat released from gas phase combustion that is deposited directly back to the solid	Unitless
u_i	The average velocity of the combined gas in direction i at a given location	Distance/time
θ	The average potential temperature of the combined gas at a given location	Temperature
x_i	The spatial unit of distance in the i direction	Distance
R_{ij}	The Reynolds stress tensor	Unitless
g_i	The acceleration of gravity in the i direction	Distance/(time)^2
C_D	The drag coefficient	Unitless
s_s	The size scale of the local solid structures	Distance
$\rho_{wood(micro)}$	The microscopic density of wood	Mass/volume